SOIL Discuss., 2, 1345–1391, 2015
www.soil-discuss.net/2/1345/2015/
doi:10.5194/soild-2-1345-2015

SOIL Discussions Open Access EGU

Arctic soil development on a series of marine terraces on Central Spitsbergen, Svalbard: a combined geochronology, fieldwork and modelling approach

W. M. van der Meij[1,2], A. J. A. M. Temme[2,3], C. M. F. J. J. de Kleijn[2], T. Reimann[2], G. B. M. Heuvelink[2], Z. Zwoliński[4], G. Rachlewicz[4], K. Rymer[4], and M. Sommer[1,5]

[1]Leibniz Centre for Agricultural Landscape Research (ZALF) e.V., Institute of Soil Landscape Research, Eberswalder Straße 84, 15374 Müncheberg, Germany
[2]Soil Geography and Landscape group, Wageningen University, P.O. Box 47, Wageningen, the Netherlands
[3]Institute for Alpine and Arctic Research (INSTAAR), University of Colorado, Boulder, Colorado, USA
[4]Institute of Geoecology and Geoinformation, Adam Mickiewicz University, Poznań, Poland
[5]Institute of Earth and Environmental Sciences, University of Potsdam, 14476 Potsdam, Germany

Received: 30 October 2015 – Accepted: 21 November 2015 – Published: 17 December 2015
Correspondence to: W. M. van der Meij (marijn.vandermeij@wur.nl)
Published by Copernicus Publications on behalf of the European Geosciences Union.

SOILD
2, 1345–1391, 2015

Abstract

Soils in Arctic regions currently enjoy significant attention because of their potentially substantial changes under climate change. It is important to quantify the natural processes and rates of development of these soils, to better define and determine current and future changes. Specifically, there is a need to quantify the interactions between various landscape and soil forming processes that together have resulted in current soil properties. Soil chronosequences are ideal natural experiments for this purpose. In this contribution, we combine field observations, luminescence dating and soil-landscape modelling to test and improve our understanding about Arctic soil formation. Our field site is a Holocene chronosequence of gravelly raised marine terraces in central Spitsbergen.

Field observations suggest that soil-landscape development is mainly driven by weathering, silt translocation, aeolian deposition and rill erosion. Spatial soil heterogeneity is mainly caused by soil age, morphological position and depth under the surface. Substantial organic matter accumulation only occurs in few, badly drained positions. Luminescence dating confirmed existing radiocarbon dating of the terraces, which are between ~3.6 and ~14.4 ka old. Observations and ages were used to parameterize soil landscape evolution model LORICA, which was subsequently used to test the hypothesis that our field-observed processes indeed dominate soil-landscape development. Model results indicate the importance of aeolian deposition as a source of fine material in the subsoil for both sheltered beach trough positions and barren beach ridge positions. Simulated overland erosion was negligible. Therefore, an un-simulated process must be responsible for creating the observed erosion rills. Dissolution and physical weathering both play a major role. However, by using present day soil observations, relative physical and chemical weathering could not be disentangled. Discrepancies between field and model results indicate that soil formation is non-linear and driven by spatially and temporally varying boundary conditions which were not included in the model. Concluding, Arctic soil and landscape

SOILD

2, 1345–1391, 2015

development appears to be more complex and less straight-forward than could be reasoned from field observations.

1 Introduction

Soils in Arctic and boreal landscapes have recently raised intense research interest. This is because the climate in these regions is expected to experience stronger changes than elsewhere (e.g. Arctic Climate Impact Assessment, 2004; Forland et al., 2011; Zwoliński et al., 2008). The effects of this increase are so far only partially understood (e.g. plant community development, Hodkinson et al., 2003). Another point of interest in the area is the poorly constrained Arctic carbon pool and its potential as carbon sink (e.g. Ping et al., 2008). To provide context to the short-term changes (~ 100 years) in Arctic and boreal soils that we are currently observing, knowledge on long-term soil development (~ 10 000 years) is urgently required as baseline. This suggests that we need to better constrain the natural (i.e. paraglacial, Ballantyne, 2002; Slaymaker, 2011) processes, rates and feedbacks in the soil-landscape system. With such understanding, meaningful comparisons can be made between short-term rates of change in soils due to changing climate on one hand, and long-term rates of change in soils on the other hand.

Chronosequences are a popular means to obtain information about natural rates of soil formation (e.g. Birkeland, 1992; Egli et al., 2006; Phillips, 2015; Sommer and Schlichting, 1997). In chronosequences, differences in properties of soils are attributed to differences in the age of those soils. This attribution is valid if other soil forming processes, such as landscape position, climate, lithology or organisms, do not vary between positions on the chronosequence. Ideally (but unusually), these factors are also constant over time. In Arctic regions, two paraglacial landscape settings are particularly suitable for chronosequences. Proglacial areas, where glaciers are currently retreating, are often used to compare soils formed at the onset of the recent retreat (~ 100 years ago) with those formed in very recently exposed glacial parent

SOILD
2, 1345–1391, 2015

material. This can provide decadal rates of soil formation (Egli et al., 2014; Kabala and Zapart, 2012). Another successful chronosequence setting is provided by series of marine terraces, also known as raised beaches, reflecting millennial-scale isostatic rebound after the end of the Last Glacial Maximum. Such terraces are ubiquitous in Arctic landscapes (Scheffers et al., 2012). Terrace chronosequences can provide millennial rates of soil formation, which is particularly helpful because natural soil formation in Arctic regions is relatively slow and many differences become apparent only after thousands of years.

Several factors nonetheless complicate the use of marine terraces to study rates of natural soil formation. First, a typical terrace consists of slight elevated ridge positions and somewhat lower trough positions and thus contains altitude differences resulting in different hydrological conditions that affect soil formation (Makaske and Augustinus, 1998; Scheffers et al., 2012). Second, geomorphic processes may not only have a different effect on ridges and troughs, but also on terraces on different positions in the landscape – particularly when a marine terrace complex is part of otherwise mountainous topography. Erosion and deposition can occur with different rates on different terrace levels. Third, it is difficult to verify whether the composition and particle size distribution of soil parent material (beach deposits) at the onset of soil formation have been the same within and between terrace levels. In other words, the soil forming factors landscape position and parent material are not the same in all positions of the chronosequence. These complications to chronosequences can lead to a problem of attribution: are observed differences between soils predominantly the result of a difference in age, or are other factors important as well?

The attribution problem can only be solved by using a combination of various methods. Clearly, geochronology is needed to provide accurate dating of the initiation of soil formation, and field and laboratory observations of soils are needed to determine properties of interest. However, in addition to these methods, model simulations of the various effects of age and other soil forming factors on soil development in a landscape

SOILD
2, 1345–1391, 2015

context are needed to determine which differences in soil forming factors may have caused differences in observations.

In this study, we focused on soils in a sequence of marine terraces in central Spitsbergen, Svalbard archipelago, to derive natural processes and rates of soil formation in a landscape context (Elster and Rachlewicz, 2012; Rachlewicz et al., 2013; Zwoliński et al., 2013). We first used Optically Stimulated Luminescence (OSL) dating to complement earlier experimental datings of juvenile marine shells on the same series of terraces (Long et al., 2012). Then, we performed field and laboratory analyses to describe soil properties in a variety of locations on the marine terrace complex. Together with dating results, this allowed us to calculate rates of some soil forming processes. Third, we used these rates to simulate combined soil-landscape development using a spatially distributed soil-landscape evolution model. Soil-landscape modelling has hitherto rarely been used in soil chronosequence studies (but see Sauer et al., 2012). However, by combining the various interacting geomorphic and pedogenic process, it allowed us to test and increase our understanding of interacting soil and landscape shaping processes in the study site. For simulations, we first hypothesized which soil-forming processes played a dominant role. Next, the recently developed soil-landscape evolution model LORICA (Temme and Vanwalleghem, 2015) was adapted to reflect this hypothesis. Model inputs and parameters were derived from field observations. Model outputs were compared to observations and conclusions were drawn with regard to the validity of our hypotheses.

2 Study area

2.1 Location and geomorphology

Fieldwork was conducted in the Ebba valley, one of the glacial valleys that enter Petunia Bay in the north tip of the Billefjorden, Central Spitsbergen (Svalbard archipelago, Fig. 1). A sequence of six marine terraces is located at the mouth of the valley, bordered

SOILD
2, 1345–1391, 2015

by the Ebba river and floodplain to the north, alluvial material to the east and south and by the fjord to the west. Prominent erosion rills and tundra lakes were excluded from the study area (Fig. 1). The terrace sediments (i.e. soil parent material) dominantly consist of well-rounded gravel and coarse sand of limestone lithology, but gravel and sand from shale, sandstone and mafic intrusions are also found.

The area has been subject of research for many years (e.g. Gulińska et al., 2003; Kłysz et al., 1988, 1989; Long et al., 2012; Zwoliński et al., 2013). The marine terraces occupy a range of altitudes in the landscape, due to isostatic rebound after the last Glacial. The oldest terrace level in the Ebba valley is even older and dates back to the Late Pleistocene (> 37 000 years). It is located on the flanks of the mountain range south-east of the study area (Kłysz et al., 1989) The typical, smooth ridge and trough morphology (Makaske and Augustinus, 1998; Scheffers et al., 2012) of terraces was formed by wave-action and sea-level fluctuations. Six Holocene terrace levels can be distinguished, each consisting of a smaller series of ridges and intermediate troughs. The oldest marine terrace in this series (terrace 6, Fig. 1) is very small and was not sampled in the present study. There are no marine terraces younger than about 3000 years due to current relative sea level rise (Rachlewicz et al., 2013). Several lower terraces have been dated using an experimental approach of radiocarbon dating of juvenile marine shells (Long et al., 2012). The authors mentioned that a source of uncertainty in this method is the possibility of dating shells older than the terrace ridge they were found on. However, quality of their datings concurred to the more common method of radiocarbon dating of driftwood. Ages showed a clear trend with altitude.

Due to their slightly more sheltered position and lower altitude relative to the smooth ridges, the troughs reveal denser vegetation. Ridge positions are in general free from vegetation. In the aerial photograph, the barren ridges and terrace edges are characterized by lighter colours, whereas trough positions are characterized by darker colours (Fig. 1)

SOILD
2, 1345–1391, 2015

2.2 Arctic soils

Most soils of Spitsbergen have formed in coastal settings. Soils typically have shallow profiles with poorly differentiated genetic horizons, sandy or loamy texture, pH-values varying between 7 and 8 and organic carbon contents from 0 up to 4 % (Melke and Chodorowski, 2006; Pereverzev, 2012). In some cases, soils have been affected by geomorphic activity such as cryogenic processes and erosion (Lindner and Marks, 1990). Thickness of marine deposits is between 1 and 2 m (Zwoliński et al., 2013). Soils formed in those deposits are well developed compared to proglacial soils, but are nonetheless mainly described as incompletely developed soils (Cambisols, Cryosols, Leptosols, Regosols, Kabala and Zapart, 2009).

The dominantly mentioned soil forming processes are: weathering through frost action and dissolution (Forman and Miller, 1984; Kabala and Zapart, 2009), calcification (Courty et al., 1994; Ugolini, 1986), silt eluviation (Forman and Miller, 1984) and the formation of organic matter (Melke, 2007).

2.3 Climate

The study area has an average annual temperature of −5 °C, with average temperatures in summer and winter of +6 and −15 °C respectively (Przybylak et al., 2014). The average annual precipitation is 150–200 mm, mainly as snow fall (Láska et al., 2012; Rachlewicz and Szczuciński, 2008; Rachlewicz et al., 2013). The climatic conditions are more extreme compared to the western coast of Spitsbergen, with warmer summers, colder winters and general aridity (Przybylak et al., 2014; Rachlewicz, 2009). The climate is classified as an Arctic Desert or Tundra (ET, Köppen, 1931).

The prevailing wind directions in the Ebba valley are south or northeast with the strongest winds ($> 6\,m\,s^{-1}$) blowing from the Ebba glacier in the northeast (Láska et al., 2012). These strong winds in combination with scarce vegetation and a high availability of sediments on the sandur plains leads to active wind erosion and

SOILD
2, 1345–1391, 2015

eventually to accumulation of aeolian sediments. Deposition occurs when wind speed decreases or when the sediments get mixed with falling snow in autumn and winter, also known as niveo-aeolian deposition (Rachlewicz, 2010). In the Ebba valley plants are a good indicator of hydrological and soil characteristics, yet reflect the cold climate. Hydrophilic species are found in wet trough positions whereas vascular species were found on better drained and better developed soils on ridges (Jónsdóttir et al., 2006; Prach et al., 2012). Vegetation cover in the study area is around 30 % (Buchwal et al., 2013).

3 Methods

3.1 Luminescence dating

To complement the experimental rebound chronology from Long et al. (2012), we applied OSL dating to samples of marine sediments from terrace levels 1, 3 and 5 in the study area (Fig. 1). Two quantities are determined for OSL dating. First, measurement of the OSL signal on the purified quartz mineral fraction reveals how much ionizing radiation the sample received since the last bleaching event (i.e. prior to burial). Second, this measurement is combined with a measurement of the background radiation level at the sample position. The luminescence age (ka) is then obtained by dividing the amount of radiation received (palaeodose, Gy) by the rate at which this dose accumulates (dose rate, $\mathrm{Gy\,ka^{-1}}$):

$$\text{OSL age (ka)} = \text{Palaeodose (Gy)}/\text{dose rate (Gy\,ka}^{-1}\text{)}. \quad (1)$$

The basic principles of OSL dating are reviewed in Aitken (1998) and Preusser et al. (2008).

For dose rate estimation we used high-resolution gamma ray spectrometry. Activity concentrations of ^{40}K and several nuclides from the Uranium and Thorium decay chains were measured. Results were combined with information on geographic location and

SOILD
2, 1345–1391, 2015

burial history (Prescott and Hutton, 1994), water and organic content history (Aitken, 1998; Madsen et al., 2005). Furthermore, grain size dependent attenuation effects were incorporated (Mejdahl, 1979) to calculate the effective dose rate. The total dose rate is listed in Table 2.

For the OSL measurements the three sediment samples were prepared in the Netherlands Centre for Luminescence dating under subdued orange light conditions. The samples were sieved to obtain the 180–250 µm grain size fractions which were subsequently cleaned using HCl (10 %) and H_20_2 (10 %). Grains of different minerals were separated from each other using a heavy liquid (LST). The quartz-rich fraction ($\rho > 2.58\,g\,cm^{-3}$) was then etched with 40 % HF for 45 min to remove remaining feldspar contamination and the outer rim of the quartz grains. The purified quartz fraction was again sieved with a 180 µm mesh to remove particles that had become too small by etching.

To estimate the palaeodose of the samples, the OSL from quartz was measured by applying the single-aliquot regenerative-dose (SAR) measurement protocol of Murray and Wintle (2003). The most light-sensitive and most suitable OSL signal of the quartz grains was selected using the "Early Background" approach (Cunningham and Wallinga, 2010). To obtain a good estimate of the palaeodose, measurements were repeated on at least 28 subsamples (aliquots) per sample. Each aliquot consisted of 40–70 grains. To test the SAR procedure, a dose recovery experiment was carried out on four aliquots of each sample. The average recovered dose agreed with the laboratory given dose. The ratio of measured dose divided by given laboratory dose was 0.96 ± 0.02 ($n = 11$) confirming the suitability of the selected measurement parameters.

The single-aliquot palaeodose distributions were symmetric and moderately scattered. We calculated over-dispersion values, i.e. the scatter in the palaeodose distributions that cannot be explained by the measurement uncertainties (Galbraith et al., 1999), to be between 12 ± 3 and 33 ± 9 %. These over-dispersion values are typical for well-bleached sediments derived from coarse-grained marine deposits (e.g.

SOILD
2, 1345–1391, 2015

Reimann et al., 2012). Therefore, palaeodoses of our samples were derived from the single-aliquot palaeodose distributions by applying the Central Age Model (CAM, Galbraith et al., 1999).

3.2 Soil observations

The study area was divided into three equally sized strata based on altitude, which in turn were divided into vegetated (trough) and non-vegetated (ridge) sub-strata using the aerial photograph from summer 2009. Thirty random locations were divided over the six strata according to stratum size, with at least 2 locations in each stratum (Fig. 1). 11 pits were located on ridge positions and 19 pits on trough positions.

Soil profiles were described according to FAO standards (FAO, 2006; IUSS Working Group WRB, 2014). Additionally, the B/ classification as proposed by Forman and Miller (1984), was used for layers with substantial silt illuviation. To easily distinguish between different parent materials, aeolian horizons were recorded with the prefix 1, whereas horizons developed in parent marine material were recorded with the prefix 2. This was done even when marine material was not overlain by aeolian material (Fig. 4).

We classified soils purely based on field observations. In most (well drained) positions, this meant that we were unable to determine whether the conditions for a Cryic horizon were met. In these cases, we assumed horizons were not Cryic.

Soil pits were dug until the unaltered parent material was reached or until further digging was not possible. Each major soil horizon was sampled. Bulk density was measured in the field using a 100 cm^3 bulk density ring. For horizons with predominantly gravel, it was not always possible to completely fill the ring by hammering it into the soil. In these cases, the bulk density ring was manually filled up with soil material, which may have led to an underestimation of bulk density. Field bulk density measurements were corrected for the moisture content, which was determined by drying samples overnight at 105 °C. Samples were subsequently dry sieved into three grain size fractions: gravel (> 2 mm), sand (2–0.063 mm) and silt and

SOILD
2, 1345–1391, 2015

clay (< 0.063 mm). Organic matter content was determined by loss on ignition. Samples were heated to 550 °C for 3 h.

The effects of soil horizon, terrace level and terrace morphological setting (ridge/trough) on the soil properties were assessed using a three-factor analysis of variance (ANOVA). A linear model was used to explain variation using the three factors.

3.3 Soilscape model LORICA

Soilscape model LORICA was used to simulate joint soil and landscape development. This raster-based model simulates lateral geomorphic surface processes together with vertical soil development (Temme and Vanwalleghem, 2015, Fig. 2). Transport and change of sediments and soil material are based on a mass balance of various grain size classes.

The model setup that was used in this study contained 10 soil layers in every raster cell of 10 m × 10 m, each with an initial thickness of 0.15 m. This created an initial thickness of marine sediments (the soil parent material) of 1.5 m. Only three grain size classes were simulated: gravel (> 2 mm), sand (2–0.063 mm) and the combined silt and clay class, from now on called silt (< 0.063 mm).

During model simulations, the different processes can change the mass of material in each grain size class in each soil layer. Using a bulk density pedotransfer function, this change in mass and composition of soil material is translated to a change in layer thickness and a corresponding change in surface altitude. Geomorphic processes only affect the top layer of each cell, while soil forming processes alter and transport material in a vertical direction between layers.

Some of LORICA's original soil process formulations were adapted to match our hypothesis of the main processes occurring in marine terraces. Some other processes were assumed less relevant, based on literature and exploratory fieldwork. Hence, they were deactivated for this study.

Chemical weathering was also not activated. However, it is important to note that chemical weathering in the form of dissolution does occur in the marine terraces

SOILD
2, 1345–1391, 2015

(Mazurek et al., 2012) and constitutes a source of sand and silt in Arctic soils elsewhere (reported from the west of Spitsbergen, Forman and Miller, 1984; Ugolini, 1986). However, it is not clear to which extent dissolution contributes to in situ weathering on the marine terraces specifically, where physical weathering also plays a dominant role. Only physical weathering was activated in LORICA. Since dissolution mainly focuses on fine material (Courty et al., 1994), a possible overestimation of the finer fractions, relative to the coarse fractions, would be an indicator of the importance, and possibly the rate, of dissolution.

3.3.1 Model framework

A DEM with a cell size of 10 m × 10 m served as input landscape. For trough positions, the thickness of the 1A horizon following from a trend with age was subtracted from the DEM to simulate initial conditions. A part of the upslope area was included in the DEM to enable import of sediments into the study area. Climatic data required by LORICA are precipitation and evapotranspiration. As we did not have data on the paleoclimate of the study area, we assumed a constant precipitation and evapotranspiration over the entire model run. The same goes for rates and parameters of the simulated processes (Table 1). Annual precipitation is approximately 200 mm (Rachlewicz, 2009; Rachlewicz et al., 2013; Strzelecki, 2012). We assumed that a large fraction is lost to infiltration, evapotranspiration and sublimation, leaving 50 mm for overland flow. The initial composition of the marine parent material was derived from field observations and is 90 % gravel with 10 % sand.

To reflect isostatic rebound, a growing part of the landscape was exposed to process calculations as time progressed. Results from geochronology of marine terraces were used to inform this. Simulations started at the time when terrace level 6 was completely above water and progressed with an annual timestep. Cells outside the study area (Fig. 1) were not included in simulations.

The activated processes and modifications to them are described below. Where applicable, the calculation of parameter values is also described.

SOILD
2, 1345–1391, 2015

3.3.2 Geomorphic processes

LORICA generates run–off and infiltration by applying precipitation and snow melt to the grid cells. Run–off flows downhill, potentially eroding and collecting sediment on its way. When the amount of transported sediment surpasses the sediment transport capacity of the water, deposition starts. Sediments can be transported out of the study area to the Ebba river and Petunia bay. Vegetation protection and surface armouring by coarse grains decrease the mass of material that can be eroded. A more extensive explanation of this landscape process is provided in Temme and Vanwalleghem (2015). Standard parameter values were used for almost all parameters describing this process, except for the vegetation protection constant. This dimensionless parameter was set from 1 to 0.5 because of the scarce vegetation in the study site.

For aeolian deposition, a simple linear process description was implemented that added a constant amount of aeolian material to all cells in trough positions for every timestep. Ridge positions received no aeolian deposition. The aerial photograph (Fig. 1), aggregated to the raster cell size of the input DEM of 10 m, was used to distinguish between ridge and trough positions.

The annual volume of aeolian deposition per cell surface ($m^3\,m^{-2}\,y^{-1}$, or $m\,y^{-1}$) was calculated by regressing observed aeolian (1A) horizon thickness to soil age. Bulk density of aeolian deposits, undisturbed by current vegetation, was measured in the field and used to convert the volume to mass. The initial grain size distribution of aeolian deposits was calculated by extrapolating trends in sand and silt fractions of 1A horizons with age to timestep 0.

3.3.3 Pedogenic processes

Pedotransfer functions are used to estimate unknown variables from readily available soil data (McBratney et al., 2002). Because LORICA's original pedotransfer function for bulk density (BD_f, $kg\,m^{-3}$) is unsuitable for clast-supported soils, we estimated a new pedotransfer function based on the gravel and sand fractions and depth under

SOILD
2, 1345–1391, 2015

the soil surface of a soil layer. Soil horizons from both marine and aeolian parent material, where bulk density and particle size distribution were known ($n = 62$), were used to estimate the parameters of this function (Eq. 2). The pedotransfer function was validated using leave-one-out cross-validation on the 62 soil horizons (RMSE = 183 kg m^{-3}, $R^2 = 0.25$).

$$\mathrm{BD}_l = 99 + 1212 \cdot \mathrm{gravel}_{\mathrm{frac},l} + 1283 \cdot \mathrm{sand}_{\mathrm{frac},l} + 353 \cdot \mathrm{depth}_l. \quad (2)$$

Physical weathering in LORICA for the various grain size classes i is described as:

$$\Delta M_{\mathrm{pw}i,l} = -M_{i,l} C_3 e C_4 \mathrm{depth}_l \frac{C_5}{\log \mathrm{size}_i}, \quad (3)$$

where the change in mass due to physical weathering ΔM_{pw} in layer l is a function of the mass present in the grain size class $M_{i,l}$, depth below the surface depth_l and the median grain size of the fraction size_i (Temme and Vanwalleghem, 2015). With parameter C_5 at its standard value of 5, weathering increases with increasing grain size. Weathering rate C_3 and depth-decay parameter C_4 were parameterized from field data.

To calculate these parameters, we assumed that a change in gravel fraction in the subsoil is only due to physical weathering. In contrast, topsoil horizons were assumed to be also affected by geomorphic processes. First, weathering rate C of gravel in 2B/ and 2BC horizons was derived from the decay in gravel fraction using:

$$\log(\mathrm{gravel}_{t,l}) = \log(\mathrm{gravel}_{0,l}) \cdot C_{\mathrm{gravel},l} \cdot t \quad (4)$$

with $\mathrm{gravel}_{t,l}$, $\mathrm{gravel}_{0,l}$ and $C_{\mathrm{gravel},l}$ as gravel fraction at time t (–), initial gravel fraction (–) and weathering rate of gravel in horizon l (y^{-1}) respectively.

Second, depth decay parameter C_4 was derived using the differences in weathering rates and average depths between the B/ and BC horizons.

With the depth decay constant C_4, the weathering rate at the soil surface ($C_{\mathrm{gravel},0}$) was derived, and weathering rate C_3 was calculated using Eq. (3).

SOILD
2, 1345–1391, 2015

Silt translocation was simulated using LORICA's formulation for clay eluviation (Temme and Vanwalleghem, 2015), but a depth decay factor was introduced to better simulate the belly shape of the silt profiles in the soil.

The values for the maximum silt eluviation in a completely silty sediment, and the depth decay factor were determined using manual inverse modelling (i.e. through model calibration), using 40 runs with different parameter values. Simulated silt profiles were compared with observed silt profiles for four representative soil profiles in the field (profiles 3, 6, 10 and 24). The objective function for calibration was to minimize the average root mean squared error between the modelled and simulated silt fraction for 5 cm thick layers over the entire depth of the profile.

3.4 Model validation

Model results were validated using site- and horizon-specific field observations of the gravel, sand and silt fraction, matched to their respective location in the simulated soilscape. Because of the small amount of observations, also observations used for parameterization and calibration were used in the validation. These observations were used for only one of the processes, whereas validation happens over the results from all processes simulated together.

The mean prediction error (ME) was calculated to assess a bias between field measurements and model results. The root mean squared error (RMSE) was calculated to measure the difference. Normalized ME (ME_n) and RMSE ($RMSE_n$) were calculated by dividing the ME and RMSE by the average observed value (Janssen and Heuberger, 1995). For the mass fractions this was done for every profile, over the depth of observations available for that profile. For the mass content this was done by considering locations on a certain morphological position together.

SOILD
2, 1345–1391, 2015

4 Results

4.1 Geochronology

The three OSL samples taken in the marine sediments show increasing age with increasing terrace level (Figs. 1, 3, Table 2). Datings of the first main terrace level show an age of 4.4 ± 0.2 ka. The highest part of terrace level 3 has been dated to 7.3 ± 0.4 ka. Terrace level 5 dates back to 12.8 ± 1.1 ka.

These results support the radiocarbon datings of Long et al. (2012) that covered terrace levels 1–4 (Fig. 1). The combined sets of ages show a clear relation with altitude (Fig. 3). This trend, 229 years for every meter of uplift, was used to inform isostatic rebound in LORICA (Fig. 3). The offset of the regression suggests that the youngest soils that are older than the present beach, are approximately 3630 years old. The youngest soils on terrace level 6 are approximately 14 393 years old. This age was hence used as the start of our model simulations, where terrace level 6 was completely above water.

4.2 Soil types and properties

Ridge and trough positions show distinct soil types. Ridge positions are generally well drained and therefore usually contain Episkeletic Calcisols (observed 9 times), unless at a more moist position, where they developed into Skeletic Turbic Cryosols (2). Soils in a beach trough are often Endoskeletic Rendzic Cryosols (11), unless they are atypically dry (Skeletic Calcisols (2) or atypically wet (Abruptic Phaeozems (2). In the oldest terraces, trough soils are Abruptic Chernozems (4), created by bacterial and fungal breakdown of organic material, which is later transported through the soil. Trough soils are typically vegetated and therefore capture aeolian sediment which forms into an aeolian A-horizon, which is rarely present on ridges (Fig. 4).

In general, sand and OM fraction decrease towards deeper lying horizons. OM shows small variation, considering the standard deviation. Silt fraction shows a maximum

SOILD
2, 1345–1391, 2015

in 2A horizons, and afterwards decreases with increasing depth. Consequently, the relative amount of gravel increases (Table 3). Carbonate content also increases with depth. Aeolian horizons are moderately calcareous. Conversely, gravelly marine horizons appear to be extremely calcareous, while the finer textured 2A horizons show a moderate to strong $CaCO_3$ content, which indicates loss of carbonates. The fine 1A horizons show a relatively high bulk density, compared to 2A horizons. Average bulk densities increase with depth in marine sediments. The detailed field descriptions show a large variation in BD inside 1A horizons. Buried aeolian deposits, without observed humus content, have a bulk density of $1651 \pm 240\,kg\,m^{-3}$.

Nonetheless, part of the variation within soil profiles is explained by soil horizon and terrace level (Fig. 5). The three-factor ANOVA confirms the significant effect ($P < 0.05$) of the soil horizon and terrace level, as well as morphological setting on the variation in gravel and sand fraction. On the contrary, terrace level was not a significant explanatory variable for variation in silt and organic matter fraction. Here only soil horizon and morphological setting were significant in explaining part of the observed variation. A linear model involving all three factors resulted in adjusted R^2 of 0.83, 0.85, 0.42 and 0.51 for gravel, sand, silt and organic matter fraction respectively.

4.3 Process parameters

Slope of the linear regression between 1A horizon thickness and age is $1.89 \times 10^{-5}\,m\,y^{-1}$ ($R^2 = 0.29$). Multiplying this with bulk density of buried aeolian material gives a deposition rate of $0.031\,kg\,m^{-2}\,y^{-1}$. Initial sand and silt fraction of the aeolian deposits are 84 and 16 % respectively.

The weathering rate of gravel at the surface ($C_{gravel,0}$) is $4.06 \times 10^{-5}\,kg\,kg^{-1}\,y^{-1}$. This corresponds to a weathering rate of $1.26 \times 10^{-5}\,kg\,kg^{-1}\,y^{-1}$, when considering the size-dependent correction factor. The corresponding depth decay constant C_4 is $-2.22\,m^{-1}$, which means that weathering rate decreases with about 90 % per meter under the soil surface.

SOILD
2, 1345–1391, 2015

Calibration of silt eluviation resulted in a maximum eluviation of 0.15 $kg\,y^{-1}$ and a depth decay factor of 6 m^{-1}.

4.4 Simulated landscape and soils

Model results show that the only significant changes in altitude besides uplift are due to aeolian deposition, with a maximum deposition of 0.45 m, divided over 1A horizons of max ~0.3 m and silt that eluviated from them into lower horizons, contributing the other ~0.15 m. Changes in altitude caused by bulk density changes due to physical weathering are maximum 0.01 m. Simulated altitude change due to erosion and sedimentation is negligible, with amounts of several millimetres. Altitude changes are larger on older terraces. There is a clear distinction between changes for trough and ridge positions, because the latter did not receive aeolian input (Fig. 6).

Variation in simulated profile curves of different particle sizes is mainly caused by morphological position of the soils (Fig. 7). Although the general shapes of these profiles correspond with the mean observed profiles, observed profile curves show a larger spread than simulated profile curves. Observed gravel fractions are lower than simulated fractions. Sand and silt fractions and mass were larger in the field than in the model results (Fig. 8). The silt fraction in the top soils on both ridge and trough positions is higher in the field than in the model results.

Most accurate predictions for sand and silt fractions and contents are for trough positions (Table 4, Fig. 8). For gravel, ridge positions are predicted most accurate. The relatively high $RMSE_n$s indicate that there is a large spread between modelled and observed mass fractions and contents (cf. Fig. 7). On the other hand, ME_ns indicate a low bias in some of the predictions. Examples are sand and silt properties in trough positions, gravel properties in ridge positions and total mass of soil material in all positions. The positive ME_n for total mass of the soil shows that the model slightly overestimates the amount of material in the soil. Sand and silt masses and fractions are generally underestimated.

SOILD
2, 1345–1391, 2015

In some places, the morphological position as derived from the aggregated aerial photograph and used in the model differs from field-observed morphological position. These "mixed" positions (Table 4, Fig. 8) show the highest differences between observations and simulations and cause the largest errors in the validation statistics. Small differences between RMSE and ME for the mixed positions indicate that the largest part of the error is systematic, and a relatively small part is caused by a random error.

5 Discussion

5.1 Geochronology and isostatic rebound

Our new OSL dates and the existing calibrated radiocarbon results from Long et al. (2012) show comparable results for the ages of marine terraces in our study area. The combined set of ages can be rather well approximated through a linear relation with altitude above current sea level, which gives an average uplift rate of 4.4 mm y^{-1} (R^2 = 0.966, Fig. 3). The nearby Kapp Eckholm (location 23 in Forman et al., 2004) shows an average uplift rate over the last 9000 years of 5 mm y^{-1}. This is in the same order of magnitude as the average uplift rate found in this study. However, Kapp Eckholm shows a large decrease in uplift rates, from 12.5 mm y^{-1} (9000–7000 years ago) to 2 mm y^{-1} (5000 years to present). This was not apparent in our data. On the contrary, when considered individually, each set of dates suggests an increasing uplift rate over time. This provides an interesting counterpoint to the clear slowing down and reversal of uplift rates observed over all of Svalbard (Forman et al., 2004). The minimum age of the terraces of ~3.6 ka corresponds to the initiation of tide-water glaciers between 4 and 3 ka ago – in response to the Holocene cooling, which eventually led to the Little Ice Age (Svendsen and Mangerud, 1997). Apparently the uplift in the Ebba valley did slow down and eventually stop in response to renewed glacier growth. The

SOILD
2, 1345–1391, 2015

terraces formed during decreased uplift rates could have been submerged again by renewed isostatic depression and late Holocene sea level rise (Zwoliński et al., 2013).

OSL ages have in general a larger uncertainty interval than the radiocarbon ages (Fig. 3), because OSL methods provide a lower precision than radiocarbon dating, especially in the age range of interest for this study. The typical OSL uncertainty is 5–10 % for the 1-sigma confidence interval (~ 65 %), which was also achieved for the samples under investigation. However, OSL provides direct depositional ages of sand-sized marine deposits and can be used to independently validate the radiocarbon chronology. In our case both data sets agree and thus support each other.

A well-known disadvantage of radiocarbon dating is that older ages (> 35 cal ka) can easily be underestimated by contamination with more modern carbon (Briant and Bateman, 2009). This may be the case with the radiocarbon dating of the highest terrace in the Ebba valley (> 37 000 years ago, Kłysz et al., 1989), but is unlikely for the Holocene terrace sequence that was studied in this paper. More importantly, radiocarbon ages derived from marine fauna (e.g. shells) needs to be corrected for the marine reservoir effect. However, this correction does not only require extra analysis (e.g. Long et al., 2012), it typically also shows a large regional variety and thus potential bias. Another common problem of radiocarbon dating, especially in our geomorphological very dynamic setting, is re-working of the dated material (e.g. Long et al., 2012). In this case the radiocarbon age might potentially overestimate the deposition of the marine terrace. OSL does not suffer from these potential malign effects. On the other hand, OSL has already been successfully used to date recent coastal dynamics (Ballarini et al., 2003; Reimann et al., 2010) and aeolian activity (e.g. Sevink et al., 2013). Thus when considering chronosequences with a longer age span and where recent geomorphic activity plays a role, OSL is a good way to validate radiocarbon chronologies and is a powerful alternative dating method.

SOILD
2, 1345–1391, 2015

5.2 Landscape evolution

It was our intention to use the LORICA model to test our hypotheses about the combined evolution of soils and landscapes in the study area. The aspects that were not well simulated, can therefore suggest improvements to process understanding.

The main geomorphic aspect that was not well simulated, is the presence of small rills incising into the smooth terrace ridges (Mazurek et al., 2012). These were observed on all terrace levels, but not simulated (Figs. 1, 6). Model tests indicate that unrealistic erodibility values would have to be adopted to simulate the amounts of erosion that lead to rill formation in the gravelly soil material under the dry climate in the study site. This suggests that the process that has led to rill formation is not included in the model. We suggest two possible processes. First, the presence of groundwater not far under the surface, which, when frozen, can act as an impermeable layer. Combination of seeping groundwater and overland flow at ridge escarpments can then disaggregate coarse material and remove fine material (Higgins and Osterkamp, 1990). This seepage erosion occurs in cliffs and riverbanks (Fox et al., 2007; Higgins and Osterkamp, 1990), but has, to our knowledge, not been described for marine terrace sequences. Second, occasional heavy storms and high tides in the period soon after uplift above sea level may have caused temporary flooding of a beach trough that was already protected by a beach ridge. Drainage of the trough after a storm passes can have formed the rills. Both processes fit with the observed absence of a clear relation between rill size and age: the conditions that initiate rill erosion would be most prevalent after limited uplift over sea level.

Although these erosion rills occur in most of the terrace boundaries, most water is currently drained parallel to the ridges, towards the tundra lakes. These again drain to the Ebba river or the Petunia bay. Because the flow velocity through these lakes is very low, no erosion occurs.

The rate of aeolian deposition was estimated from observations without model simulations. However, a complicating factor is that this was based on present soil

SOILD
2, 1345–1391, 2015

properties: the rate of aeolian deposition was based on current thickness of aeolian cover. Ultimately, part of the silt was translocated from the simulated from the simulated aeolian deposits to deeper layers, resulting in an underestimation of thickness of 1A horizons. This effect is visible for instance in the overestimation of gravel and underestimation of sand in the top parts of profiles in trough positions (Fig. 8).

The regression between thickness of 1A horizons and age shows that age only explains a small part of variation in 1A horizon thickness. This indicates that other factors such as the initial topography, wind shadows, hydrological properties, variation in vegetation cover and reworking of aeolian sediments (e.g. Paluszkiewicz, 2003), which were not considered in our model, also play a role.

The spatial heterogeneity of aeolian deposition is visible in shorter-term measurements in the study area. Deposition during the summer periods of 2012–2014 ranged from 3 to 1713 $g\,m^{-2}$ $summerseason^{-1}$ (Rymer, 2015), while niveo-aeolian deposition in the years 2000–2005 ranged between 70 and 115 $g\,m^{-2}\,y^{-1}$ (Rachlewicz, 2010). In comparison, aeolian deposition in Hornsund, southern Spitsbergen, was 300–400 $g\,m^{-2}\,y^{-1}$ for the winter of 1957/58 (Czeppe and Jagielloński, 1966). The higher numbers in these measured ranges are about an order of magnitude larger than the average deposition rates found by aeolian horizon observation (31 $g\,m^{-2}\,y^{-1}$). Part of this difference can be caused by reworking of short-term deposits over time by continued aeolian activity, another by our underestimation of the thickness of aeolian deposits by observing them after some of the silt has eluviated from them. On top of the spatial heterogeneity, there is also a large temporal variation in niveo-aeolian deposition rates (Christiansen, 1998).

5.3 Soil formation

Both physical and chemical weathering in the Arctic are driven by moisture availability (Hall et al., 2002). Consequently, weathering occurs at a faster rate in the wetter troughs of the terraces. This expected spatial variation in weathering was observed in particle size distributions (Fig. 7), but not quantified in the model, due to data limitations. Next to

SOILD
2, 1345–1391, 2015

that, also the ANOVA indicates the significant role of morphological position on gravel, sand and silt fraction. However, it should be noted that silt is also significantly influenced by influx of aeolian deposits.

The weathering rate was calculated based on the gravel fraction of the subsurface horizons – not of the surface horizon. This was done in an attempt to exclude the effect of other processes on grain size changes. Nonetheless, dissolution (chemical weathering), which mainly reduces the silt fraction (Courty et al., 1994), may have affected grain sizes in the subsurface. Less fine material in the subsurface of older soils means more coarse material, which subsequently results in an underestimation of physical weathering rates. More, independent observations would be needed to disentangle the effects of physical and chemical weathering.

Consequently, the calculated weathering rate must be considered a combined physical and chemical weathering rate. This rate of $4.06 \times 10^{-5}\,\mathrm{kg\,kg^{-1}\,y^{-1}}$ ($4.06 \times 10^{-3}\,\%\,\mathrm{y^{-1}}$) is orders of magnitudes lower than in field weathering experiments of the dominantly chemical weathering of granite and dolomite in Swedish Lapland (Dixon et al., 2001; Thorn et al., 2002). These resulted in a weight loss of 0.121 and $0.326\,\%\,\mathrm{y^{-1}}$ respectively for an experiment of 5 years. Two reasons for this difference present themselves: time-decreasing weathering rates and moisture availability. Weathering rates decrease with time, amongst others due to precipitation of secondary minerals which slow the dissolution process (Langman et al., 2015). These secondary minerals were observed in Ebba valley, partially coating gravel (c.f. Courty et al., 1994). It is also likely that long term weathering rates in Swedish Lapland exceed those found in the Ebba valley because of the much larger precipitation ($1750\,\mathrm{mm\,y^{-1}}$, Dixon et al., 2001). Other weathering studies also indicate the dominant control of moisture in determining both physical and chemical weathering rates (e.g. Egli et al., 2015; Hall et al., 2002; Matsuoka, 1990; Wu, 2016; Yokoyama and Matsukura, 2006).

It can be argued that dissolution is a significant process in our marine terraces. This is also apparent in the field observations. 2A horizons have a lower $CaCO_3$ content than 2B, 2B/ and 2BC horizons. This is consistent with observations elsewhere in

SOILD
2, 1345–1391, 2015

Spitsbergen of a more active dissolution regime in near surface horizons, compared to subsurface horizons (Courty et al., 1994; Forman and Miller, 1984). Dissolution mainly occurs in the fine soil mass due to its larger reactive surface. Consequently, the fine fraction in 1A and 2A horizons consists of less $CaCO_3$.

Dissolution was not included in model simulations. This should have caused overestimation of fine material in the model output. However, model results instead show lower sand and silt contents than observed (Figs. 7, 8, Table 4). For trough positions, this is partly due to underestimation of the thickness of 1A horizons (see above). By this underestimation, the thinner 1A horizons give way to underlying marine deposits in the model outputs. Their higher gravel content distorts the comparison between observed and simulated profiles, leading to an underestimation of sand content and fraction. Silt properties are not influenced by this error, as the eluviation rate was calibrated using valley positions. As a consequence, silt predictions there show a low error.

This disturbance by a wrongly estimated thickness of the aeolian cover is not present in ridge positions. However, also for those positions sand and silt contents are underestimated. Simulated silt content shows the largest deviation from field observations (Fig. 8, Table 4). This indicates that there is another source of sand and silt in ridge positions.

One source of silt is in situ weathering of coarse material into finer material (Fahey and Dagesse, 1984; Forman and Miller, 1984). Another source is an ex situ one, namely aeolian deposition. This is observed in trough positions, which display a higher silt fraction throughout the whole profile, compared to ridge positions (Fig. 7). The heterogeneous deposition of aeolian material over trough positions on the area has resulted in an even heterogeneous silt source for the subsurface. Hence, the ANOVA shows no significant relation between age and silt fraction.

Deposition occurs partly through entrapment with falling snow (Rachlewicz, 2010). Meltwater from this snow partly infiltrates in the permeable gravelly soils. This downward flow of water can transport part of the silt it had captured, increasing the

SOILD
2, 1345–1391, 2015

silt fraction in the subsurface. This process can also act as a source of silt in ridge positions. Material left behind on the surface can be reworked by strong summer winds, leaving no trace of aeolian deposits on these positions. This theory contradicts the observations of Forman and Miller (1984), who claim that silt in their studied marine ridges on western Spitsbergen mainly originates from in situ frost weathering and dissolution. They attribute this to absence of a major source area, absence of silt on the surface and absence of vegetation to entrap sediments. In the Ebba valley, the proglacial sandur plain acts as a major sediment source. Next to that, our observations of 2A horizons, which partly reach the surface, show high amounts of silt compared to lower lying horizons (Table 3). Due to these different conditions in the Ebba valley, it is possible that ridge positions also profit from aeolian silt input. This also can explain the deficit of silt in model simulations (Fig. 7).

Addition of a depth decay function in the simulation of silt translocation proved to result in simulated profiles comparable to the observed profiles (Fig. 7). This decay in eluviation rate with depth represents the limited water flux in the subsurface. Due to a shallow unfrozen soil in the snow melt season, the water cannot reach deeply into the soil and starts to flow laterally. Later in the season, when the active layer is thawed, the water flux is limited, because precipitation is very limited.

5.4 Temporal and spatial soil-landscape interactions

The variation in simulated soil profiles is smaller than the variation in observed soil profiles (Fig. 7). We presume that this is due to a variation in boundary conditions that is not captured in the model. Particularly, in reality, the grain size distribution of the original parent material will differ between locations, and aeolian deposition rates vary both in space and time. Next to that, temporal variation in climate is not considered. The glacial retreat since the beginning of the Holocene indicates the general warming climate in Svalbard, which also includes several colder episodes (e.g. Svendsen and Mangerud, 1997). The effects of these changing temperatures on process rates such as weathering rates were not included in the model. Precipitation and evaporation

SOILD
2, 1345–1391, 2015

rates were also not constant during the Holocene. Courty et al. (1994) show that characteristics of secondary carbonates on subsurface clasts indicate different climatic and biogenic episodes. Although their research was conducted on western Spitsbergen which has a much wetter climate than central Spitsbergen, it is likely that such variations in climate occurred over the complete Svalbard archipelago.

The elevation differences between ridges and troughs in the study area are the main driving force for spatial soil heterogeneity. Water flow accumulates in the relatively sheltered trough positions. Consequently, weathering occurs at a faster rate and there is a bit more plant growth. These plants capture a part of the aeolian sediment that has been deposited with freshly fallen snow. The resulting 1A horizon, consisting of finer material, holds more water than the marine sediments, resulting in more plant growth. This feedback has resulted in local aeolian covers of up to 70 cm. Note that this process is not expected to continue over longer timescales, because the aeolian sediments will ultimately grow out of their sheltered and, more importantly, humid positions, becoming susceptible to reworking by wind erosion.

Ultimately, Arctic soil development is not as straightforward as we hypothesized in the beginning of this paper. The interplay between different processes, known and unknown, together with variations in initial and boundary conditions in soil and landscape development has resulted in a complex soil-landscape system. Additional research is required to further unravel soil and landscape development in this fragile environment, especially in the context of a changing climate.

6 Conclusions

This study combined different methods to study soil development on a series of marine terraces in Central Spitsbergen. The analysis of the combined results of these methods led to the following conclusions:

– The gravelly soils on the marine terraces display clear effects of different soil forming processes such as physical (frost action) and chemical weathering

SOILD
2, 1345–1391, 2015

(dissolution) and translocation of silt. Dissolution mainly occurs in A horizons developed in marine material. Translocation of silt occurs everywhere in the landscape, following the water flow.

– Optically Stimulated Luminescence dating (OSL) appears to be a good method for dating isostatic uplift rates of the marine terraces. Its results confirm radiocarbon dates from the area. Combining these datings with field observations enabled the calculation of process rates using field observations.

– However, determining historical rates of weathering and aeolian deposition using current soil properties is difficult when multiple processes have influenced those properties. Especially dissolution, which removes material from the soil, distorts the mass balance of soil constituents that was used to calculate rates.

– Simulation of soil development in a landscape context with soilscape evolution model LORICA was successful in terms of simulating trends in soil properties. However, there were significant discrepancies between field observations and model results. The larger variation in field observations than in model simulations is likely mainly due to spatially and temporally varying boundary conditions that were not included in simulations. More importantly, bias in model outcomes helped to increase our understanding of Arctic soil development in the marine terraces.

– Soil development is heavily influenced by geomorphic processes, mainly aeolian deposition. Deposition acts as a source of fine material, which mainly accumulates in relatively sheltered beach trough positions. However, our results are consistent with suggestions that aeolian silt has also been added to soils in beach ridge positions. Erosion of overland flow plays a minor role, compared to erosion by extruding groundwater or by the effects of storms on young terraces.

SOILD
2, 1345–1391, 2015

Author contributions. This paper is based on the master thesis research of W. M. van der Meij and C. M. F. J. J. de Kleijn, under supervision of A. J. A. M. Temme and G. B. M. Heuvelink. Fieldwork was performed by W. M. van der Meij and C. M. F. J. J. de Kleijn at the Adam Mickiewicz University Polar Station (AMUPS), facilitated by Z. Zwoliński and G. Rachlewicz. Fieldwork was supported by K. Rymer. T. Reimann performed the OSL analysis. W. M. van der Meij and A. J. A. M. Temme adjusted the model code and W. M. van der Meij performed the simulations. M. Sommer provided conceptual pedological context and funding for the first author to work on the paper. The manuscript has been prepared by the first three authors with contributions from all other authors.

Acknowledgements. W. M. van der Meij, A. J. A. M. Temme and C. M. F. J. J. de Kleijn are grateful to the colleagues of the Adam Mickiewicz University for the opportunity of performing fieldwork at their Arctic research station. We acknowledge dr. Bart Makaske for fruitful discussions about beach morphology nomenclature. G. Rachlewicz and K. Rymer were supported by Polish National Science Centre grant no. 2011/03/B/ST10/06172.

References

Aitken, M. J.: An introduction to optical dating: the dating of Quaternary sediments by the use of photon-stimulated luminescence, Oxford University Press, UK, 1998.

Arctic Climate Impact Assessment: Impacts of a Warming Arctic – Arctic Climate Impact Assessment, Cambridge University Press, Cambridge, UK, 2004.

Ballantyne, C. K.: Paraglacial geomorphology, Quaternary Sci. Rev., 21, 1935–2017, 2002.

Ballarini, M., Wallinga, J., Murray, A., Van Heteren, S., Oost, A., Bos, A., and Van Eijk, C.: Optical dating of young coastal dunes on a decadal time scale, Quaternary Sci. Rev., 22, 1011–1017, 2003.

Birkeland, P.: Quaternary soil chronosequences in various environments–extremely arid to humid tropical, Chapter 11, in: Weathering, Soils & Paleosols, edited by: Martini, I. P. and Chesworth, W., Elsevier, Amsterdam, 261–281, 1992.

Briant, R. M. and Bateman, M. D.: Luminescence dating indicates radiocarbon age underestimation in late Pleistocene fluvial deposits from eastern England, J. Quaternary Sci., 24, 916–927, 2009.

SOILD

2, 1345–1391, 2015

Buchwal, A., Rachlewicz, G., Fonti, P., Cherubini, P., and Gärtner, H.: Temperature modulates intra-plant growth of Salix polaris from a high Arctic site (Svalbard), Polar Biol., 36, 1305–1318, 2013.
Christiansen, H. H.: "Little Ice Age" nivation activity in northeast Greenland, The Holocene, 8, 719–728, 1998.
Courty, M. A., Marlin, C., Dever, L., Tremblay, P., and Vachier, P.: The properties, genesis and environmental significance of calcitic pendents from the High Arctic (Spitsbergen), Geoderma, 61, 71–102, 1994.
Cunningham, A. C. and Wallinga, J.: Selection of integration time intervals for quartz OSL decay curves, Quat. Geochronol., 5, 657–666, 2010.
Czeppe, Z. and Jagielloński, U.: Przebieg głównych procesów morfogenetycznych w południowo-zachodnim Spitsbergenie, Uniwersytet Jagielloński, Kraków, Poland, 1966.
Dixon, J. C., Thorn, C. E., Darmody, R. G., and Schlyter, P.: Weathering rates of fine pebbles at the soil surface in Kärkevagge, Swedish Lapland, Catena, 45, 273–286, 2001.
Egli, M., Wernli, M., Kneisel, C., and Haeberli, W.: Melting glaciers and soil development in the proglacial area Morteratsch (Swiss Alps): I. Soil type chronosequence, Arct. Antarct. Alp. Res., 38, 499–509, 2006.
Egli, M., Dahms, D., and Norton, K.: Soil formation rates on silicate parent material in alpine environments: Different approaches-different results?, Geoderma, 213, 320–333, 2014.
Egli, M., Lessovaia, S. N., Chistyakov, K., Inozemzev, S., Polekhovsky, Y., and Ganyushkin, D.: Microclimate affects soil chemical and mineralogical properties of cold alpine soils of the Altai Mountains (Russia), J. Soil. Sediment., 15, 1420–1436, 2015.
Elster, J. and Rachlewicz, G.: Petuniabukta, Billefjorden in Svalbard: Czech–Polish long term ecological and geographical research, Pol. Polar Res., 33, 289–295, 2012.
Fahey, B. D. and Dagesse, D. F.: An experimental study of the effect of humidity and temperature variations on the granular disintegration of argillaceous carbonate rocks in cold climates, Arct. Antarct. Alp. Res., 16, 291–298, 1984.
FAO: Guidelines for soil description, Rome, 2006.
Forland, E. J., Benestad, R., Hanssen-Bauer, I., Haugen, J. E., and Skaugen, T. E.: Temperature and Precipitation Development at Svalbard 1900–2100, Advances in Meteorology, 2011, 893790, doi:10.1155/2011/893790, 2011.

SOILD
2, 1345–1391, 2015

Forman, S. L. and Miller, G. H.: Time-dependent soil morphologies and pedogenic processes on raised beaches, Broggerhalvoya, Spitsbergen, Svalbard archipelago, Arct. Antarct. Alp. Res., 16, 381–394, 1984.

Forman, S. L., Lubinski, D. J., Ingólfsson, Ó., Zeeberg, J. J., Snyder, J. A., Siegert, M. J., and Matishov, G. G.: A review of postglacial emergence on Svalbard, Franz Josef Land and Novaya Zemlya, northern Eurasia, Quaternary Sci. Rev., 23, 1391–1434, 2004.

Fox, G. A., Wilson, G. V., Simon, A., Langendoen, E. J., Akay, O., and Fuchs, J. W.: Measuring streambank erosion due to ground water seepage: correlation to bank pore water pressure, precipitation and stream stage, Earth Surf. Proc. Land., 32, 1558–1573, 2007.

Galbraith, R. F., Roberts, R. G., Laslett, G., Yoshida, H., and Olley, J. M.: Optical dating of single and multiple grains of quartz from Jinmium rock shelter, Northern Australia: Part I, experimental design and statistical models, Archaeometry, 41, 339–364, 1999.

Gulińska, J., Rachlewicz, G., Szczuciński, W., Barałkiewicz, D., Kózka, M., Bulska, E., and Burzyk, M.: Soil contamination in high Arctic areas of human impact, central Spitsbergen, Svalbard, Pol. J. Environ. Stud., 12, 701–707, 2003.

Hall, K., Thorn, C. E., Matsuoka, N., and Prick, A.: Weathering in cold regions: some thoughts and perspectives, Prog. Phys. Geog., 26, 577–603, 2002.

Higgins, C. G. and Osterkamp, W. R.: Seepage-induced cliff recession and regional denudation, Chapter 14, in: Groundwater Geomorphology: The Role of Subsurface Water in Earth-Surface Processes and Landforms, edited by: Higgins, C. G. and Coates, D. R., Geological Society of America, Boulder, Colorado, Special Paper, 252, 291–318, 1990.

Hodkinson, I. D., Coulson, S. J., and Webb, N. R.: Community assembly along proglacial chronosequences in the high Arctic: vegetation and soil development in north-west Svalbard, J. Ecol., 91, 651–663, 2003.

IUSS Working Group WRB: World Reference Base for Soil Resources 2014, International soil classification system for naming soils and creating legends for soil maps, FAO, Rome, 191 pp., 2014.

Janssen, P. and Heuberger, P.: Calibration of process-oriented models, Ecol. Model., 83, 55–66, 1995.

Jónsdóttir, I. S., Austrheim, G., and Elvebakk, A.: Exploring plant-ecological patterns at different spatial scales on Svalbard, UNIS, Longyearbyen, UNIS Publication Series, 87 pp., 2006.

Kabala, C. and Zapart, J.: Recent, relic and buried soils in the forefield of Werenskiold Glacier, SW Spitsbergen, Pol. Polar Res., 30, 161–178, 2009.

SOILD

2, 1345–1391, 2015

Kabala, C. and Zapart, J.: Initial soil development and carbon accumulation on moraines of the rapidly retreating Werenskiold Glacier, SW Spitsbergen, Svalbard archipelago, Geoderma, 175, 9–20, 2012.

Kłysz, P., Lindner, L., Makowska, A., Marks, L., and Wysokiński, L.: Late Quaternary glacial episodes and sea level changes in the northeastern Billefjorden region, Central Spitsbergen, Acta Geol. Pol., 38, 107–123, 1988.

Kłysz, P., Lindner, L., Marks, L., and Wysokiński, L.: Late Pleistocene and Holocene relief remodelling in the Ebbadalen-Nordenskióldbreen region in Olav V Land, central Spitsbergen, Pol. Polar Res., 10, 277–301, 1989.

Köppen, W. P.: Grundriss der Klimakunde, Walter de Gruyter, Berlin, 1931.

Langman, J. B., Blowes, D. W., Sinclair, S. A., Krentz, A., Amos, R. T., Smith, L. J., Pham, H. N., Sego, D. C., and Smith, L.: Early evolution of weathering and sulfide depletion of a low-sulfur, granitic, waste rock in an Arctic climate: A laboratory and field site comparison, J. Geochem. Explor., 156, 61–71, doi:10.1016/j.gexplo.2015.05.004, 2015.

Láska, K., Witoszová, D., and Prošek, P.: Weather patterns of the coastal zone of Petuniabukta, central Spitsbergen in the period 2008–2010, Pol. Polar Res., 33, 297–318, 2012.

Lindner, L. and Marks, L.: Geodynamic aspects of studies of Quaternary inland sediments in South Spitsbergen (attempt to synthesis), Pol. Polar Res., 11, 365-387, 1990.

Long, A. J., Strzelecki, M. C., Lloyd, J. M., and Bryant, C. L.: Dating High Arctic Holocene relative sea level changes using juvenile articulated marine shells in raised beaches, Quaternary Sci. Rev., 48, 61–66, 2012.

Madsen, A. T., Murray, A., Andersen, T., Pejrup, M., and Breuning-Madsen, H.: Optically stimulated luminescence dating of young estuarine sediments: a comparison with ^{210}Pb and ^{137}Cs dating, Mar. Geol., 214, 251–268, 2005.

Makaske, B. and Augustinus, P. G.: Morphologic changes of a micro-tidal, low wave energy beach face during a spring-neap tide cycle, Rhone-Delta, France, J. Coastal Res., 14, 632–645, 1998.

Matsuoka, N.: Mechanisms of rock breakdown by frost action: an experimental approach, Cold Reg. Sci. Technol., 17, 253–270, 1990.

Mazurek, M., Paluszkiewicz, R., Rachlewicz, G., and Zwoliński, Z.: Variability of water chemistry in tundra lakes, Petuniabukta coast, Central Spitsbergen, Svalbard, The Scientific World Journal, 2012, 596516, doi:10.1100/2012/596516, 2012.

SOILD
2, 1345–1391, 2015

McBratney, A. B., Minasny, B., Cattle, S. R., and Vervoort, R. W.: From pedotransfer functions to soil inference systems, Geoderma, 109, 41–73, 2002.
Mejdahl, V.: Thermoluminescence dating: Beta-dose attenuation in quartz grains, Archaeometry, 21, 61–72, 1979.
Melke, J.: Characteristics of soil filamentous fungi communities isolated from various microrelief forms in the high Arctic tundra (Bellsund region, Spitsbergen), Pol. Polar Res., 28, 57–73, 2007.
Melke, J. and Chodorowski, J.: Formation of Arctic soils in Chamberlindalen, Bellsund, Spitsbergen, Pol. Polar Res., 27, 119–132, 2006.
Murray, A. S. and Wintle, A. G.: The single aliquot regenerative dose protocol: potential for improvements in reliability, Radiat. Meas., 37, 377–381, 2003.
Paluszkiewicz, R.: Zróżnicowanie natężenia transportu eolicznego w warunkach polarnych jako efekt zmienności czynników meteorologicznych na przykładzie doliny Ebby (Petuniabukta, Billefjorden, Spitsbergen Środkowy) [Differentiation of aeolian transport intensity in polar conditions as an effect of variability in meteorological factors. Case study of the Ebba valley], in: The Functioning of Polar Ecosystems as Viewed Against Global Environmental Changes, edited by: Olech, M. A., XXIX International Polar Symposium, Kraków, 19–21 September 2003, 235–238, 2003.
Pereverzev, V. N.: Soils developed from marine and moraine Deposits on the Billefjord coast, West Spitsbergen, Eurasian Soil Science, 45, 1023–1032, 2012.
Phillips, J. D.: The robustness of chronosequences, Ecol. Model., 298, 16–23, 2015.
Ping, C.-L., Michaelson, G. J., Jorgenson, M. T., Kimble, J. M., Epstein, H., Romanovsky, V. E., and Walker, D. A.: High stocks of soil organic carbon in the North American Arctic region, Nat. Geosci., 1, 615–619, 2008.
Prach, K., Klimešová, J., Košnar, J., Redčenko, O., and Hais, M.: Variability of contemporary vegetation around Petuniabukta, central Spitsbergen, Pol. Polar Res., 33, 383–394, 2012.
Prescott, J. R. and Hutton, J. T.: Cosmic ray contributions to dose rates for luminescence and ESR dating: large depths and long-term time variations, Radiat. Meas., 23, 497–500, 1994.
Preusser, F., Degering, D., Fuchs, M., Hilgers, A., Kadereit, A., Klasen, N., Krbetschek, M., Richter, D., and Spencer, J. Q.: Luminescence dating: basics, methods and applications, Quaternary Science Journal, 57, 95–149, 2008.

SOILD
2, 1345–1391, 2015

Przybylak, R., Araźny, A., Nordli, Ø., Finkelnburg, R., Kejna, M., Budzik, T., Migała, K., Sikora, S., Puczko, D., and Rymer, K.: Spatial distribution of air temperature on Svalbard during 1 year with campaign measurements, Int. J. Climatol., 34, 3702–3719, 2014.

Rachlewicz, G.: Contemporary Sediment Fluxes and Relief Changes in High Artic Glacierized Valley Systems (Billefjorden, Central Spitsbergen), Wydawnictwo Naukowe Uniwersytetu im. Adama Mickiewicza, Poznań, 2009.

Rachlewicz, G.: Paraglacial modifications of glacial sediments over millennial to decadal time-scales in the high Arctic (Billefjorden, central Spitsbergen, Svalbard), Quaestiones Geographicae, 29, 59–67, 2010.

Rachlewicz, G. and Szczuciński, W.: Changes in thermal structure of permafrost active layer in a dry polar climate, Petuniabukta, Svalbard, Pol. Polar Res., 29, 261–278, 2008.

Rachlewicz, G., Zwoliński, Z., Kostrzewski, A., and Birkenmajer, K.: Geographical environment in the vicinity of the Adam Mickiewicz University in Poznań Polar Station–Petuniabukta, in: Ancient and Modern Geoecosystems of Spitsbergen, Polish geomorphological research, edited by: Zwoliński, Z., Kostrzewski, A., and Pulina, M., Bogucki Wydawnictwo Naukowe, Poznań, 205–243, 2013.

Reimann, T., Naumann, M., Tsukamoto, S., and Frechen, M.: Luminescence dating of coastal sediments from the Baltic Sea coastal barrier-spit Darss–Zingst, NE Germany, Geomorphology, 122, 264–273, 2010.

Reimann, T., Lindhorst, S., Thomsen, K. J., Murray, A. S., and Frechen, M.: OSL dating of mixed coastal sediment (Sylt, German Bight, North Sea), Quat. Geochronol., 11, 52–67, 2012.

Rymer, K.: The aeolian processes observations in Ebba valley (central Spitsbergen), 2010–2015 (Conference abstract), available at: http://www.polarknow.us.edu.pl/IPSiS/pdf/Pe_20.pdf (last access: 14 October 2015), 2015.

Sauer, D., Finke, P., Sørensen, R., Sperstad, R., Schülli-Maurer, I., Høeg, H., and Stahr, K.: Testing a soil development model against southern Norway soil chronosequences, Quatern. Int., 265, 18–31, 2012.

Scheffers, A., Engel, M., Scheffers, S., Squire, P., and Kelletat, D.: Beach ridge systems – archives for holocene coastal events?, Prog. Phys. Geog., 36, 5–37, 2012.

Sevink, J., Koster, E., van Geel, B., and Wallinga, J.: Drift sands, lakes, and soils: the multiphase Holocene history of the Laarder Wasmeren area near Hilversum, the Netherlands, Neth. J. Geosci., 92, 243–266, 2013.

SOILD
2, 1345–1391, 2015

Slaymaker, O.: Criteria to distinguish between periglacial, proglacial and paraglacial environments, Quaestiones Geographicae, 30, 85–94, 2011.
Sommer, M. and Schlichting, E.: Archetypes of catenas in respect to matter – a concept for structuring and grouping catenas, Geoderma, 76, 1–33, 1997.
Strzelecki, M. C.: High Arctic Paraglacial Coastal Evolution in Northern Billefjorden, Svalbard, PhD thesis, Department of Geography, Durham University, Durham, UK, 303 pp., 2012.
Svendsen, J. I. and Mangerud, J.: Holocene glacial and climatic variations on Spitsbergen, Svalbard, Holocene, 7, 45–57, 1997.
Temme, A. J. A. M. and Vanwalleghem, T.: LORICA – A new model for linking landscape and soil profile evolution: development and sensitivity analysis, Comput. Geosci., doi:10.1016/j.cageo.2015.08.004, online first, 2015.
Thorn, C. E., Darmody, R. G., Dixon, J. C., and Schlyter, P.: Weathering rates of buried machine-polished rock disks, Kärkevagge, Swedish Lapland, Earth Surf. Proc. Land., 27, 831–845, 2002.
Ugolini, F. C.: Pedogenic zonation in the well-drained soils of the Arctic regions, Quatern. Res., 26, 100–120, 1986.
Wu, W.: Hydrochemistry of inland rivers in the north Tibetan Plateau: Constraints and weathering rate estimation, Sci. Total Environ., 541, 468–482, 2016.
Yokoyama, T. and Matsukura, Y.: Field and laboratory experiments on weathering rates of granodiorite: separation of chemical and physical processes, Geology, 34, 809–812, 2006.
Zwoliński, Z., Kostrzewski, A., and Rachlewicz, G.: Environmental changes in the Arctic, in: Environmental Changes and Geomorphic Hazards, edited by: Singh, S., Starkel, L., and Syiemlieh, H. J., Bookwell, Delhi, 23–36, 2008.
Zwoliński, Z., Gizejewski, J., Karczewski, A., Kasprzak, M., Lankauf, K. R., Migon, P., Pekala, K., Repelewska-Pekalowa, J., Rachlewicz, G., Sobota, I., Stankowski, W., and Zagorski, P.: Geomorphological settings of Polish research stations on Spitsbergen, Landform Analysis, 22, 125–143, 2013.

SOILD
2, 1345–1391, 2015

Table 1. Settings and parameters used as input for the LORICA model.

General		Simulation time (years)	14 393
		Timestep (years)	1
		Number of soil layers	10
		Initial soil depth (m)	1.5
		Precipitation ($m\,y^{-1}$)	0.2
		Evapotranspiration ($m\,y^{-1}$)	0.075
		Infiltration ($m\,y^{-1}$)	0.075
	Initial composition of the soil	Gravel (%)	90
		Sand (%)	10
		Silt (%)	0
Geomorphic processes	Water erosion and deposition	p (multiple flow factor)	2
		m (exponent of overland flow)	1.67
		n (exponent of slope)	1.3
		K (erodibility)	0.0003
		Erosion threshold	0.01
		Rock protection constant	1
		Bio protection constant	0.5
		Selectivity change constant	0
Soil forming processes	Physical weathering	Weathering rate constant (y^{-1})	1.26×10^{-5}
		Depth decay constant (m^{-1})	−2.22
		Particle size constant (m)	5
	Particle size	Coarse fraction (m)	0.01
		Sand fraction (m)	0.002
		Silt fraction (m)	0.000065
	Silt translocation	Maximum eluviation (kg)	0.15
		Depth decay constant (m^{-1})	6
		Saturation constant	1

SOILD
2, 1345–1391, 2015

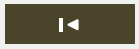

Table 2. OSL ages with uncertainty of 1σ for 3 samples taken in the study area (Fig. 1). Experimental details are provided in Sect. 3.1.

Location Fig. 1	NCL lab. code	Altitude (m)	Depth (m)	Palaeodose (Gy)	Dose rate (Gy ka^{-1})	OSL age (ka)	Systematic error (ka)	Random error (ka)
I	NCL-2114067	5.5	0.57	5.9 ± 0.2	1.34 ± 0.05	4.4 ± 0.2	0.14	0.18
II	NCL-2114068	11.1	0.27	11.8 ± 0.6	1.62 ± 0.05	7.3 ± 0.4	0.23	0.37
III	NCL-2114066	41.6	0.57	20.3 ± 1.6	1.58 ± 0.05	12.8 ± 1.1	0.41	0.97

SOILD
2, 1345–1391, 2015

Table 3. Average and standard deviation of properties of sampled horizons. Horizons with errors in sampling were left out. The *n* indicates the remaining samples. Carbonate content was measured in the field according to FAO (2006).

Horizon	1A ($n = 22$)	2A ($n = 17$)	2B ($n = 4$)	2B/ ($n = 24$)	2BC ($n = 11$)
Thickness (m)	0.24 ± 0.16	0.16 ± 0.09	0.28 ± 0.08	0.32 ± 0.22	0.35 ± 0.19
Gravel (–)	0.01 ± 0.02	0.26 ± 0.27	0.70 ± 0.20	0.66 ± 0.15	0.77 ± 0.15
Sand (–)	0.89 ± 0.03	0.59 ± 0.24	0.25 ± 0.18	0.26 ± 0.12	0.20 ± 0.15
Silt (–)	0.09 ± 0.03	0.14 ± 0.07	0.04 ± 0.03	0.08 ± 0.04	0.03 ± 0.01
OM (–)	0.04 ± 0.01	0.04 ± 0.03	0.02 ± 0.02	0.01 ± 0.01	0.005 ± 0.004
$CaCO_3$ (%)	2–10	2–25	> 25	> 25	> 25
BD ($kg\,m^{-3}$)	1304 ± 176	1262 ± 184	1345 ± 103	1424 ± 131	1543 ± 377

SOILD
2, 1345–1391, 2015

Table 4. Normalized RMSE and ME as validation statistics of the model results, ordered per geomorphic position. Mixed positions are locations where the model follows a different geomorphological setting than was observed in the field. This is due to loss of details with aggregation of the ridge-trough map to the cell size of the input DEM.

		Statistic	Trough	Ridge	Mixed	Total
Gravel	Fraction	ME_n	1.683	0.118	3.829	1.931
		$RMSE_n$	2.381	0.223	4.181	2.443
	Mass	ME_n	0.320	0.129	1.354	0.433
		$RMSE_n$	0.579	0.174	2.064	0.809
Sand	Fraction	ME_n	−0.135	0.429	−0.341	−0.087
		$RMSE_n$	0.517	0.975	0.830	0.672
	Mass	ME_n	−0.202	0.010	−0.555	−0.305
		$RMSE_n$	0.410	0.488	0.845	0.653
Silt	Fraction	ME_n	−0.043	−0.652	−0.375	−0.228
		$RMSE_n$	0.744	1.005	0.914	0.830
	Mass	ME_n	−0.060	−0.670	−0.579	−0.299
		$RMSE_n$	0.383	0.863	0.988	0.690
All sizes	Fraction	ME_n	0	0	0	0
		$RMSE_n$	0.638	0.320	1.033	0.679
	Mass	ME_n	0.024	0.063	0.042	0.038
		$RMSE_n$	0.161	0.084	0.092	0.128
Count	Fraction		17	5	7	29
	Mass		14	5	7	26

SOILD
2, 1345–1391, 2015

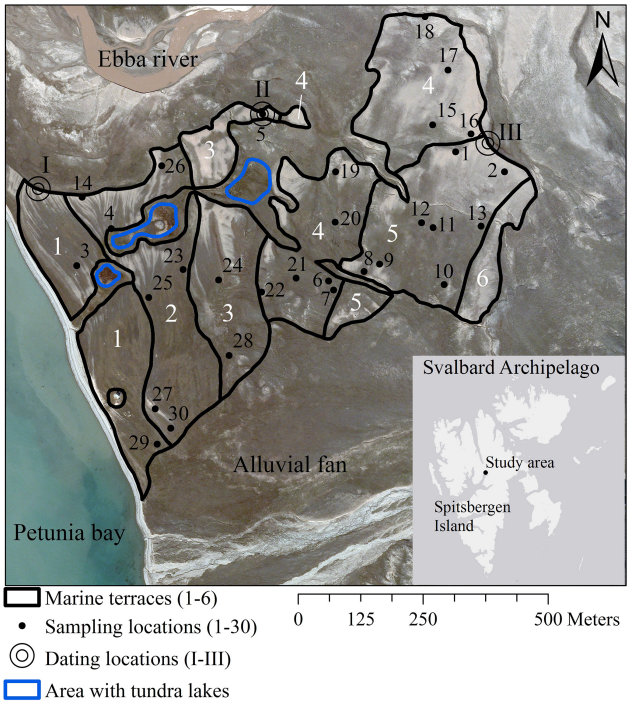

Figure 1. Aerial photograph (summer 2009) of the study area indicating the 6 terrace levels (in white numerals), 3 OSL-dating locations (in Roman numerals) and 30 sampling locations (in black numerals). Ridges are recognizable as light (un-vegetated) parts of the terraces, troughs are darker (vegetated). Disturbed areas such as erosion rills, permanently wet depressions and tundra lakes were excluded from the study area. The inset shows the location of the study area on the Spitsbergen Island.

SOILD
2, 1345–1391, 2015

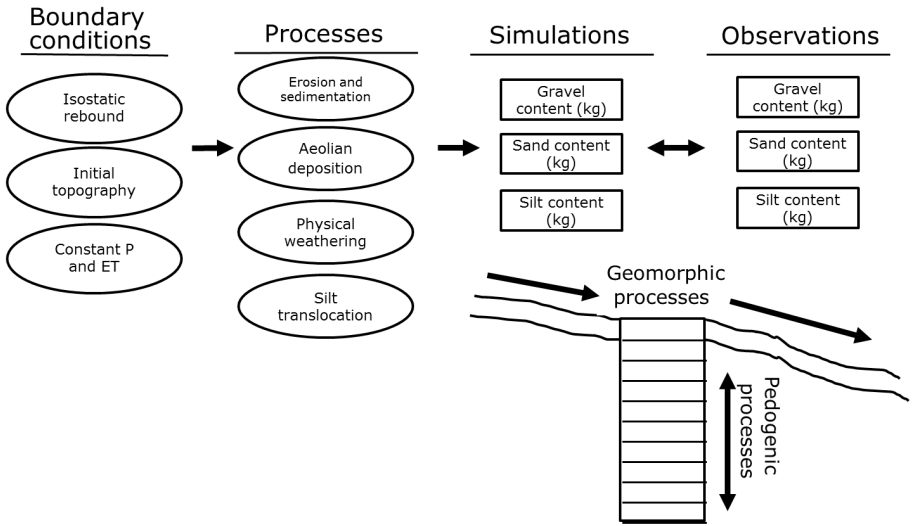

Figure 2. Conceptual framework of LORICA as used in this study.

SOILD
2, 1345–1391, 2015

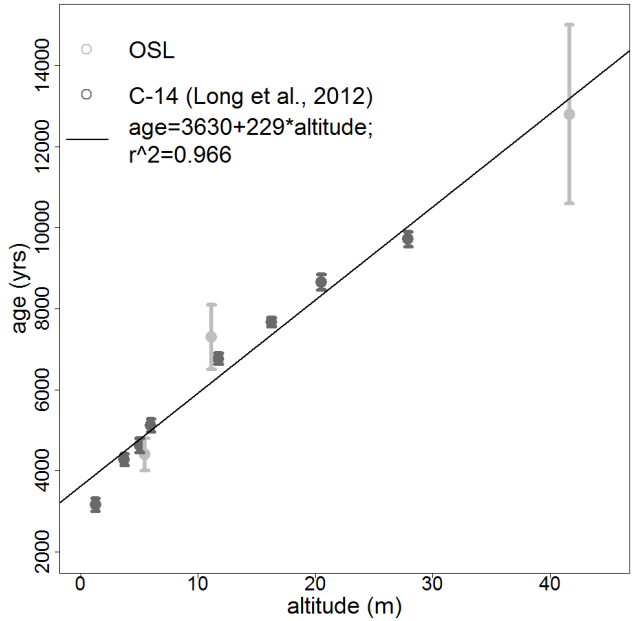

Figure 3. Elevation and age of OSL dates (this study) and radiocarbon dates (Long et al., 2012). Ages are displayed with a confidence interval of 2σ. The black line shows a regression between altitude and age of each dating.

SOILD
2, 1345–1391, 2015

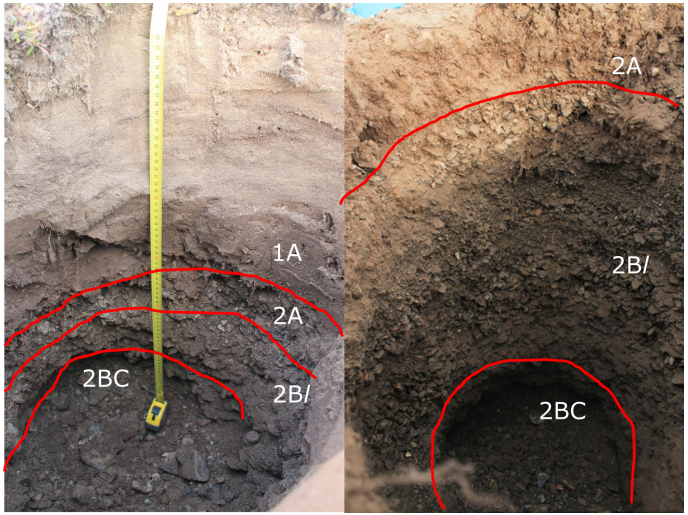

Figure 4. Examples of a typical soil found on a trough (left) and ridge location (right). The prefixed numbers indicate the parent material: aeolian (1) or marine (2).

SOILD
2, 1345–1391, 2015

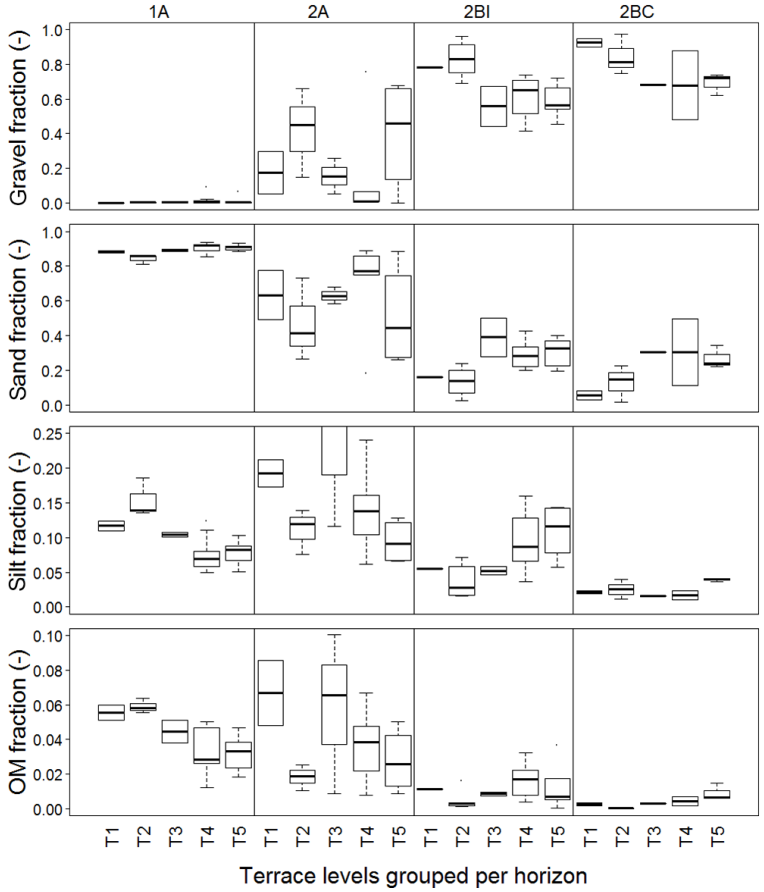

Figure 5. Boxplots of observed soil properties on different terrace levels, ordered by main soil horizon.

SOILD
2, 1345–1391, 2015

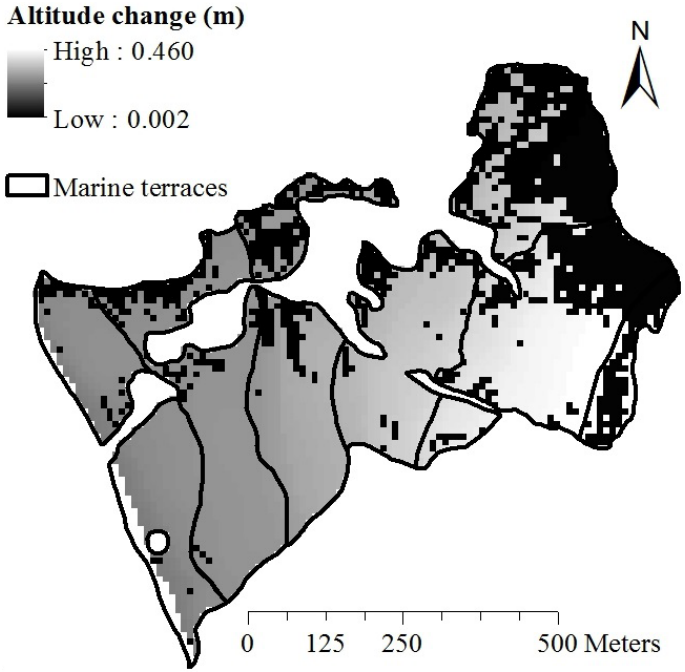

Figure 6. Simulated altitude change in the study area. A clear difference is visible between ridge positions (black grid cells) and trough positions (grey scales), due to absence of aeolian deposition on ridge positions.

SOILD
2, 1345–1391, 2015

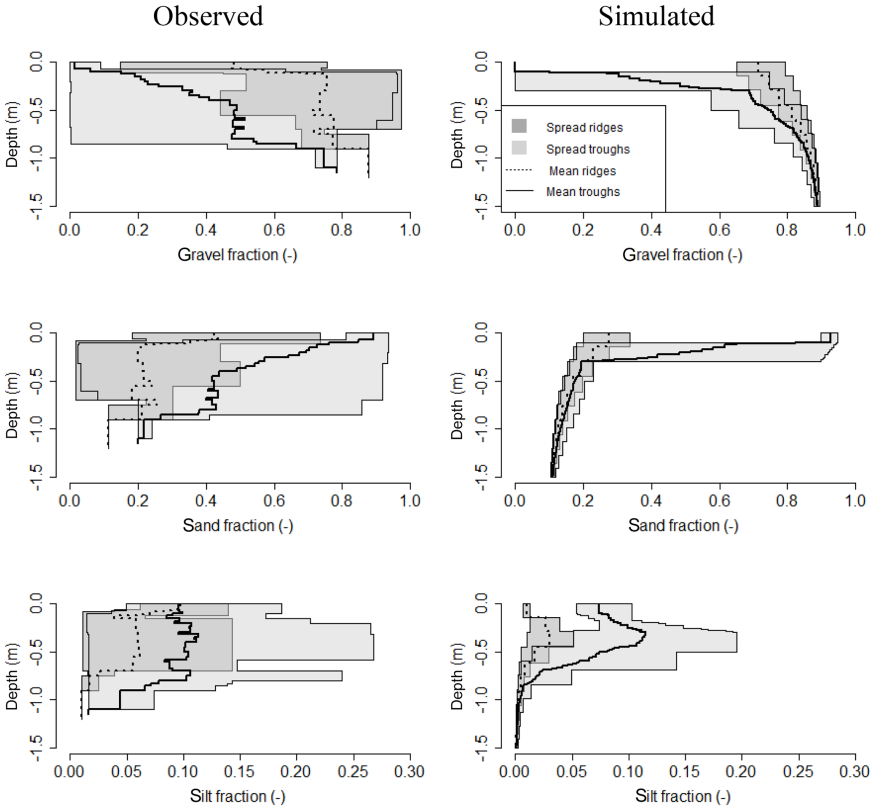

Figure 7. Total variation and mean of particle fractions in observed and modelled profile curves, divided over morphological setting. For every cm along the soil profile depth, the minimum, maximum and mean mass fraction of the various grain sizes for all profiles in the considered morphological setting are displayed.

SOILD
2, 1345–1391, 2015

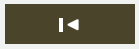

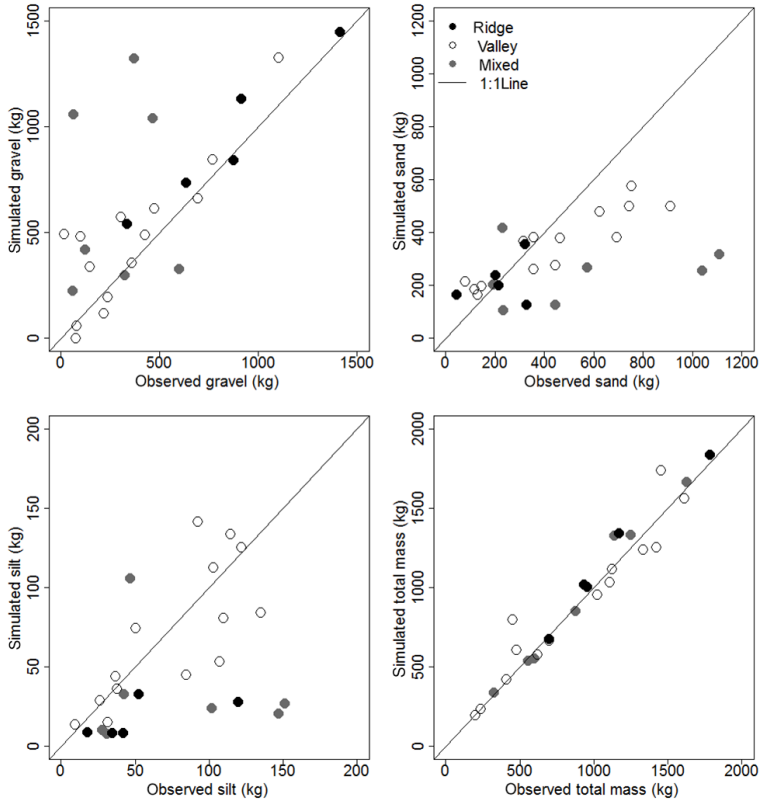

Figure 8. Scatterplots of simulated versus observed mass in kg over the total observed depth, for different particle sizes and morphological positions. The black line indicates the 1 : 1 line, which indicates a perfect match between model and field results.

SOILD
2, 1345–1391, 2015